Polymer Composites

WILEY | spe INSPIRING PLASTICS PROFESSIONALS

RESEARCH ARTICLE OPEN ACCESS

Mechanical Characterization of Fused Deposition Modeling-Printed Wood-Polylactic Acid Composites Under Water Conditioning

Weilong Xu[1] | Meiyu Li[1] | Yanan Xu[2] | Ali Entezari[3] | Jianguang Fang[1]

[1]School of Civil and Environmental Engineering, University of Technology Sydney, Sydney, New South Wales, Australia | [2]School of Aerospace, Mechanical and Mechatronic Engineering, The University of Sydney, Sydney, New South Wales, Australia | [3]School of Biomedical Engineering, University of Technology Sydney, Sydney, New South Wales, Australia

Correspondence: Jianguang Fang (jianguang.fang@uts.edu.au)

Received: 19 May 2025 | **Revised:** 10 September 2025 | **Accepted:** 12 September 2025

Funding: This work was supported by Australian Research Council (ARC) (grant no. DE210101676).

Keywords: fused deposition modeling (FDM) | moisture effect | single edged notched bending (SENB) | tensile property | wood fiber

ABSTRACT

Natural fiber-reinforced thermoplastic composites have gained increasing attention due to their sustainability. Additive manufacturing, particularly Fused Deposition Modeling (FDM), enables the fabrication of such composites with complex geometries. This study investigates the mechanical behavior of wood-polylactic acid (PLA) composites fabricated via FDM, focusing on their tensile and fracture properties under different water absorption durations. Results indicate that wood-PLA exhibits reduced tensile strength and stiffness compared to pure PLA. The tensile strength for wood-PLA was 23.4 MPa, which was significantly lower than the strength of the PLA (54.6 MPa). However, the wood-PLA showed enhanced strain energy density in the tensile test, measuring 1.41 times greater than the PLA, and higher energy absorption ability in the Single Edged Notched Bending (SENB) test. Water uptake induced plasticisation effects in the wood-PLA composites, resulting in a 20% reduction in strength and a 10% decrease in elastic modulus after 15 days. Moreover, elongation at break increased by 66%, contributing to a 48% improvement in energy absorption. Notably, these effects are reversible upon redrying, suggesting that water primarily acts as an external plasticizer. The study highlights the mechanical response of wood-PLA composites and provides insights into their structural integrity in humid environments.

1 | Introduction

Additive manufacturing (AM), also known as 3D printing, has seen increasingly widespread adoption across various fields in recent years due to its ability to fabricate complex structures with reduced material waste, labor input, and production time [1]. AM comprises various techniques, such as material extrusion (MEX), laminated object manufacturing (LOM), and vat photopolymerisation, each offering distinct process characteristics and material compatibility. Among various AM techniques, Fused Deposition Modeling (FDM) stands out for its cost-effectiveness and wide material compatibility, enabling broad applications in sectors [1] such as automotive, aerospace, construction materials, and medical devices [2–4]. In particular, FDM is commonly categorized under MEX processes and has received significant attention for thermoplastic-based applications. To further diversify the functional and structural properties of printed parts, fiber-reinforced polymer composites have been increasingly adopted in FDM printing.

The composites offer enhanced properties, such as improved biocompatibility, reduced weight, greater durability, and

Summary

- Wood-PLA exhibits lower strength but higher energy absorption than PLA.
- Wood-PLA demonstrates zig-zag fracture behavior unlike brittle PLA.
- Wood-PLA shows higher water absorption than PLA over multiple days.
- Water immersion reduces strength but increases energy absorption in wood-PLA.
- Redrying reverses moisture effects, confirming water plasticizing.

superior aesthetics, compared to single-material systems, thereby expanding their range of applications [5, 6]. Currently, the commonly used fibers include carbon fiber [7, 8], glass fiber [9, 10], and aramid fibers [11], allowing the design of application-specific components for a broad range of demanding environments.

Natural or bio-based fibers have emerged in recent years as new materials suitable for composites, frequently combined with polymers such as PLA (Polylactic Acid), TPU (Thermoplastic Polyurethane), and PA (Polyamide) to produce filaments for FDM [12–14]. Compared to traditional materials like carbon fiber, these bio-based fibers offer several advantages, including easy availability from natural sources, biodegradability, and lower carbon emissions [6]. Recent studies have begun to focus on the mechanical properties of natural fiber composites and how the other factors affect their mechanical properties, including the effects of varying fiber content [15], printing parameters [12] (such as printing thickness [16]), and the impact of additives on the optimization of their internal structure and properties [13]. Some studies have also focused on utilizing recycled raw materials to produce natural fibers, thereby enhancing their sustainability benefits. This includes the use of materials such as flax [17], potato starch [18], grains [19], short banana fibers, and recycled palm residues [20], which are blended with various types of polymers to create FDM-compatible filaments. Additionally, the high cellulose content in natural fibers results in significant water absorption [21, 22], leading to pronounced changes in performance upon moisture exposure.

Wood-PLA composites represent a unique class of natural fiber composites that simultaneously exhibit biodegradability [23, 24], good interfacial adhesion, and adaptability to FDM printing [25, 26]. Among various commercially available bio-composite filaments, it remains one of the most widely adopted natural fiber-reinforced materials for FDM applications [27]. However, a critical challenge in utilizing wood-PLA composite material is its inevitable moisture absorption in real-world environments [28]. The highly hydrophilic nature of wood fibers makes wood-PLA composites significantly more susceptible to swelling or softening [29]. These moisture-induced changes pose serious concerns for applications requiring environmental durability, such as outdoor decorative elements, biodegradable packaging [30], and functional prototypes [31, 32], which are often exposed to humid environments, temperature fluctuations, or direct water contact during their service life [33].

Numerous studies have investigated the effects of water absorption on wood-PLA composites. Ainin et al. found that wood-PLA shows significant strength loss due to the swelling and structural distortion upon immersion [34], while Ecker et al. reported more severe degradation in FDM-printed samples compared to injection-molded ones [35]. Oliver-Ortega et al. showed that PLA composites reinforced with bleached softwood fibers still exhibited moisture sensitivity due to the hydrophilic nature of the fibers [36]. Ayrilmis and his colleagues revealed that increasing wood content and layer thickness lead to higher porosity, thus reducing strength and increasing water uptake [16, 37]. Several reviews have explained these effects through fiber swelling, diffusion, and interfacial debonding [38]. Moisture diffusion in such systems is often described using Fick's law, which enables quantitative modeling of water uptake behavior. This approach has also been applied to other natural fiber-reinforced thermoplastics, such as oil palm fiber/ABS composites, revealing that as the fiber content increased, the water uptake capacity also increased, accompanied by a decrease in the diffusion coefficient (D) and an approach of the kinetic exponent (n) toward 0.5, indicating a Fickian diffusion process [39]. Martínez-Sánchez et al. highlighted the role of printing parameters in controlling moisture adsorption [40], and Zandvliet et al. noted that even for interior applications [41], PLA-based composites face dimensional instability from water exposure. Surface property studies also show compromised wettability and bonding performance as wood content increases.

Despite these findings, few studies have addressed the recovery of mechanical performance after re-drying or directly compared PLA and wood-PLA under the same aging and drying conditions. Mechanical evaluations are often limited to tensile or bending tests, lacking fracture-based insights. This study aims to address existing research gaps by investigating the mechanical performance of wood-PLA composites fabricated via FDM. Comprehensive mechanical testing was conducted to evaluate the material's response to moisture exposure and its potential for recovery after redrying. Section 2 outlines the materials and methods used in this research, detailing the fabrication process, conditioning protocols, and testing procedures. Section 3 presents the results and discussion, focusing on the comparison between PLA and wood-PLA, the effects of water absorption, and the impact of the redrying process on mechanical properties. Section 4 concludes the key findings of this study.

2 | Methods and Materials

2.1 | Materials and Samples Preparation

Two commercial filaments are involved in this research project:

1. Pure PLA, called PLA EF 3D850, with a diameter of 2.85 mm, was purchased from a commercial supplier (Nanovia, Louargat, France). The slicing software used for generating the G-code was Ultimaker Cura in this study.

The density of the filament is 1.24 g/cm^3, and the recommended extrusion temperature is from 190°C to 230°C;

2. The wood-PLA composite filament, containing 40% pine wood fiber by volume and with a diameter of 2.85 mm, was purchased from the same supplier. The density of the filament is 1.13 g/cm^3, the recommended extrusion temperature is between 210°C and 230°C.

In this study, tensile samples and single edge notched bending (SENB) samples were fabricated and tested using PLA and wood-PLA materials. Ultimaker S5 FDM printer (Ultimaker, Utrecht, Netherlands) was used to print these two materials. The printing parameters listed in Table 1 were selected based on the manufacturer-recommended settings and widely adopted practices reported in previous studies [42, 43].

The preparation process of the samples is illustrated in Figure 1. Tensile samples were Type IV, conforming to ASTM D638 specifications [44], with a thickness of 1.6 mm. To fabricate tensile samples with unidirectional filaments, a hollow square tube with dimensions of 160 mm × 160 mm × 60 mm and a thickness of 1.6 mm was printed. Type IV dog-bone tensile samples were cut from each side of the hollow tube using a laser cutter (Thunder, Melbourne, Australia) [45]. This approach ensured a smooth transition in sample dimensions, which helped to minimize stress concentration in the fillet radius area and addressed issues typically observed in directly printed samples [46, 47].

TABLE 1 | FDM printing parameters.

Printing parameters	Configurations
Layer height	0.2 mm
Line width	0.8 mm
Printing temperature	210°C
Building temperature	28°C
Bed temperature	65°C
Printing speed	35 mm/s
Fill pattern (tensile)	Concentric
Fill pattern (bending)	Line

For SENB samples, the dimensions, particularly the notch length, vary across standards due to differences in material of interest and the test objectives. In this study, an optical microscope (LEICA DM2500, Leica Microsystems, Wetzlar, Switzerland) was used to characterize the printed SENB specimens. Given that 3D printing is a relatively novel technique compared to traditional manufacturing methods, standardized guidelines specifically addressing the mechanical testing of FDM printed materials have not yet been established. Current testing practices rely on existing standards for conventional manufacturing method [48]. In this study, two notch lengths (4 and 10 mm) were selected based on ASTM D5045 standard [49] and ASTM E1820 [50], which represent testing approaches for brittle polymers and ductile metals, respectively. Although wood-PLA is polymer composite, its fracture behavior exhibits characteristics of both brittle and ductile failure depending on its composition and microstructure [51, 52].

The use of two notch lengths was intended not only to comply with established standards but also to simulate practical scenarios involving different defect severities. Specifically, the 4 mm notch represents relatively minor surface flaws or damage, whereas the 10 mm notch mimics more severe internal cracks. This allows for a more comprehensive evaluation of the material's damage tolerance under flexural loading. The sharp notches were directly incorporated into 3D models and fabricated during FDM printing. High-resolution slicing was used to minimize the notch tip radius. No fatigue pre-crack was introduced, as the aim was to compare fracture behavior and energy absorption trends rather than to measure standardized fracture toughness. All

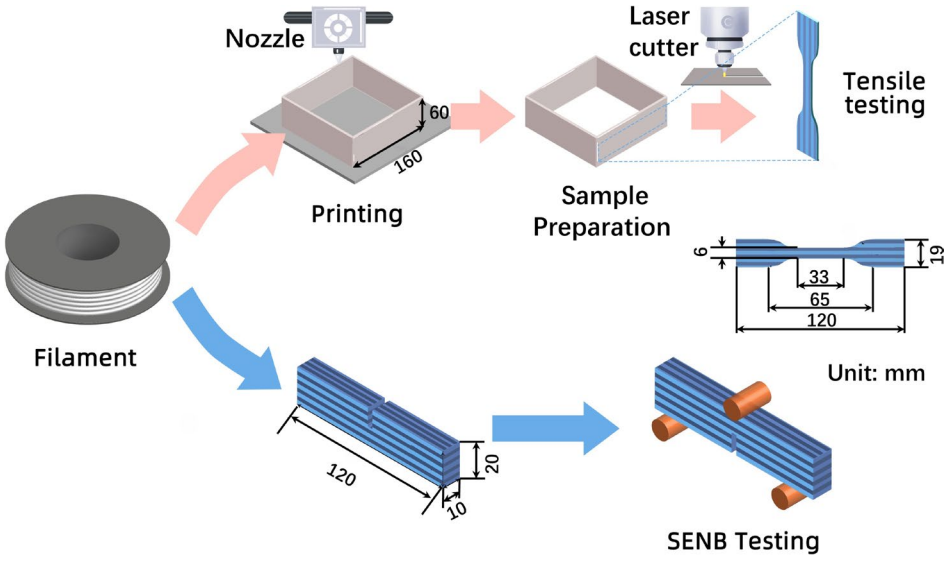

FIGURE 1 | The sample preparation processes.

SENB samples had a total length of 90 mm, a height of 20 mm, and a thickness of 10 mm.

2.2 | Water Absorption and Mechanical Testing

In this study, the effects of water absorption on the tensile and bending properties of PLA and wood-PLA materials were investigated. The experimental workflow is depicted in Figure 2. Based on the water treatment procedures, the samples were categorized into three groups: the control group, consisting of samples that were not subjected to water immersion; the wet group, comprising samples immersed in water for varying durations; and the redried group, which included samples subjected to water immersion followed by a controlled drying process. For each group, the samples were replicated in 6.

The water absorption tests were performed in accordance with ASTM D570-22 [53], with soaking water maintained at a constant room temperature of 25°C. The immersion duration was set at 3, 7, 10 and 15 days, with weight gain recorded after each period. Surface water was wiped dry with a paper towel before weighing. The water absorption rate M_t (%) was determined by:

$$M_t = \frac{W_w - W_d}{W_d} \times 100 \tag{1}$$

where W_d and W_w are the weights of dry (before immersion) and wet (after immersion) samples.

The drying process for the redried group was carried out using a vacuum desiccator with silica gel at the bottom to effectively absorb moisture. The desiccator was maintained in a temperature-controlled environment at a constant room temperature of 25°C and kept under vacuum to ensure efficient moisture removal. Each sample was dried for at least 3 days, after which the samples were weighed to verify whether their weight had returned to the initial value prior to water exposure.

Tensile and SENB tests were performed on PLA and wood-PLA samples using a universal testing machine (AGX-50kN, Shimadzu, Kyoto, Japan). The tensile tests were conducted at a constant loading speed of 2 mm/min, whereas the SENB test was performed at 4 mm/min. The experiment was considered complete when the applied load dropped to 10 N. During the experiments, the Digital Image Correlation (DIC) system was also employed to capture images and calculate strain data. Additionally, DIC images were used to generate local strain contours, providing a more detailed analysis. To ensure accurate recognition by DIC software, a sufficient amount of speckle was required on the surface of the samples. Therefore, all samples were painted to create identifiable speckle patterns.

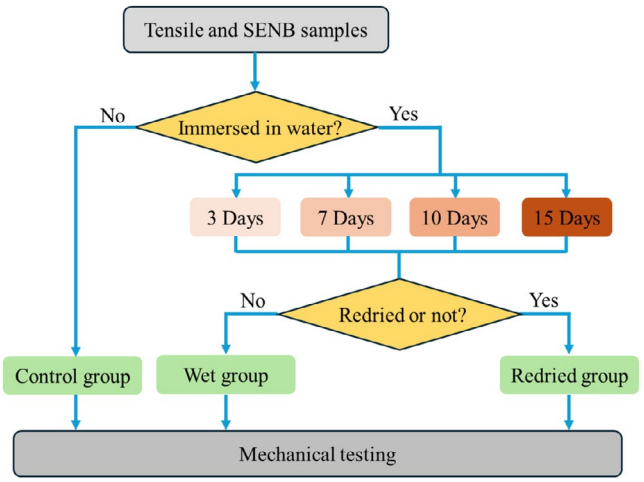

FIGURE 2 | Experimental workflow.

Stress–strain curves were obtained from tensile tests, and key mechanical parameters, including *ultimate tensile strength*, Young's modulus, elongation at break, and strain energy density, were evaluated. The strain energy density Ψ (J/m^3) is defined as the amount of energy absorbed per unit volume during the tensile test and is calculated using:

$$\Psi = \int_0^{\epsilon_{max}} \sigma d\epsilon \tag{2}$$

where σ is the stress, ϵ is the strain, and ϵ_{max} is the elongation at break.

In the data analysis, statistical methods were employed in this study, among which the Jonckheere–Terpstra method was used to examine whether the test results of the immersed samples exhibited a significant monotonic increasing or decreasing trend with immersion time [54].

In the SENB tests, energy absorption and peak force were analyzed, with energy absorption determined by the area under the force-displacement curve. The local strain was calculated using DIC images to investigate the crack initiation and propagation.

2.3 | Chemical and Thermal Characterization

To investigate the interactions between chemical bonds and the forces between polymer chains within the material, Fourier-Transform Infrared spectroscopy (FTIR) technology was employed to examine the distribution characteristics of specific functional groups, particularly hydroxyl groups [55]. FTIR spectra were recorded using a Thermo Scientific Nicolet 6700 FTIR spectrometer (Thermo Fisher Scientific, Waltham, Massachusetts, USA) equipped with an Attenuated Total Reflectance (ATR) accessory. The spectra were collected in the wavenumber range of 4000–400 cm^{-1} with a resolution of 4 cm^{-1}. A total of 32 scans were performed for each sample, and background spectra were recorded before each measurement. The samples, which were 1.6 mm thick with dimensions of 1 × 1 cm, were prepared using FDM printing. Both PLA and wood-PLA samples were scanned after complete drying treatment or after immersion in water for 15 days. The samples were directly placed on the ATR crystal for measurement. The spectra were analyzed using OMNIC software (OMNIC 9.0, Thermo Fisher Scientific, Waltham, Massachusetts, USA).

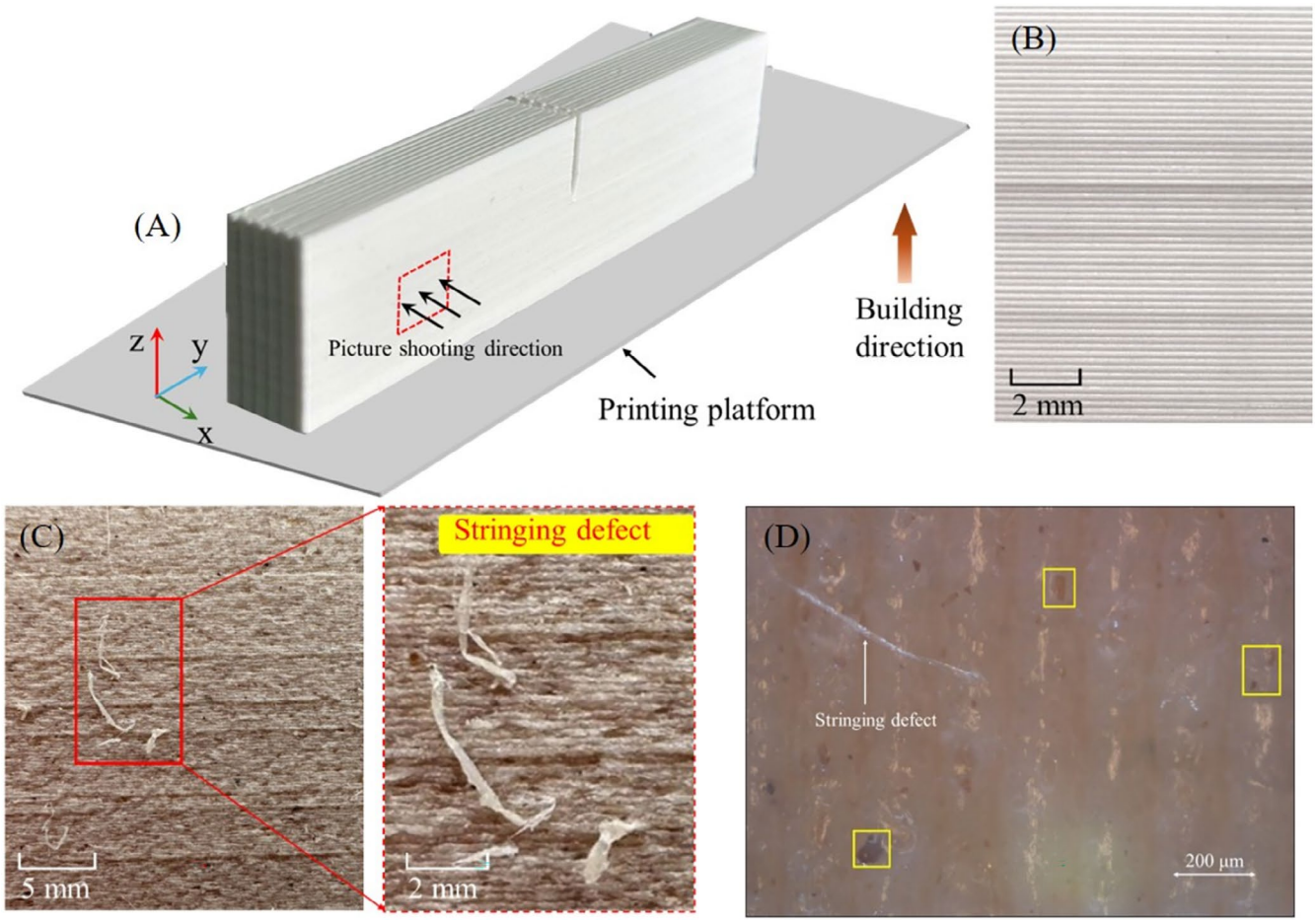

FIGURE 3 | (A) Schematic of the SENB specimen with the red frame indicating the observed region, (B) the surface of PLA and (C) wood-PLA SENB specimen, and (D) surface morphology of wood-PLA SENB specimen under an optical microscope.

Thermal analysis was conducted using a simultaneous thermal analyzer (STA 449 F1 Jupiter, Netzsch, Germany) to characterize both thermal stability and thermal transitions of the materials. Material samples were extracted from tensile specimens in the virgin group and from those in the wet group after 15 days of immersion. The material samples of approximately 6.0–9.0 mg were placed in aluminum crucibles with pierced lids. In an inert nitrogen atmosphere, these crucibles were heated to 600°C at a rate of 10°C/min. The measurements provided the glass transition temperature (T_g) from the DSC signal, as well as thermogravimetric (TG) curves and derivative thermogravimetry (DTG) reflecting the mass loss as a function of temperature.

3 | Results and Discussion

3.1 | Mechanical Properties of PLA and Wood-PLA Without Water Immersion

3.1.1 | Print Quality

Figure 3A shows a SENB specimen with the red frame marking the region for surface observation. The PLA surface exhibited a relatively smooth and uniform layer-by-layer pattern (Figure 3B). In contrast, the wood-PLA sample (Figure 3C) displayed a rough and uneven surface with noticeable stringing defects, characterized by small filaments left on the surface. The incorporation of solid wood fiber particles introduces disturbances to the melt flow field, primarily due to the disparity in flowability between the molten PLA and the non-melting fibers [56]. These disturbances, combined with the rigidity and pronounced polarity of the wood particles, further disrupt the continuity of the polymer melt phase, thereby promoting surface roughness [40]. Moreover, the potential non-uniform distribution of wood fibers can lead to spatial viscosity variations, giving rise to transient flow instabilities, pulsed extrusion behavior [57], and stringing defects [40]. Figure 3D shows the images of the surface characterization of wood-PLA captured using the optical microscope. The distribution of the wood fibers and several of their characteristics (highlighted with red dashed lines) are clearly visible, and the stringing defect is also indicated in the image.

The deviations in mass and thickness are summarized in Table 2. The nominal mass of the samples was determined by multiplying the STL-designed volume of samples by the filament density, whereas the nominal thickness corresponded to the STL-designed thickness. Both PLA and wood-PLA samples exhibited higher actual masses and thicknesses than their nominal values, indicating potential over-extrusion during printing. The deviations in the thicknesses for both materials are comparable, which is around 0.30 mm (3%), indicating good dimensional accuracy.

TABLE 2 | Deviation in mass and dimension between the printed and designed samples.

	Mass (g)			Thickness (mm)		
Sample	**Nominal**	**Actual**	**Deviation (%)**	**Nominal**	**Actual**	**Deviation (%)**
PLA	22.04	22.74 (0.29)	3.2	10	10.32 (0.11)	3.2
Wood-PLA	20.08	21.37 (0.18)	6.4	10	10.24 (0.08)	2.4

Note: Data were derived from 30 SENB samples, with standard deviation shown in parentheses.

TABLE 3 | The tensile results of PLA and wood-PLA.

Parameters	**PLA**	**Wood-PLA**
Ultimate tensile strength (MPa)	54.6 (2.44)	23.4 (1.0)
Elongation at break (%)	2.0 (0.2)	4.7 (1.0)
Young's modulus (MPa)	3074 (170)	1568 (102)
Strain energy density (10^{-7} J/m^3)	6.39 (0.9)	8.91 (1.8)

3.1.2 | Tensile Properties of PLA and Wood-PLA

Compared to pure PLA material, wood-PLA exhibited reduced ultimate tensile strength and Young's modulus. As presented in Table 3, PLA had an ultimate tensile strength of 54.6 MPa, whereas wood-PLA demonstrated a significantly lower value of 23.4 MPa, corresponding to a 57% reduction. The Young's modulus of wood-PLA was 1495 MPa, approximately 52.7% of that of PLA (3050 MPa). However, wood-PLA showed a higher elongation at break than PLA, reaching 4.7%, compared with 2.7% for PLA.

The stress–strain curves in Figure 4A show that wood-PLA exhibited a plastic deformation stage (from point II to III) after reaching its ultimate tensile strength, whereas PLA underwent brittle failure with no significant post-yield deformation. The strain distribution in Figure 4B reveals that PLA fractured immediately upon the formation of localized strain concentration in the gauge area. In contrast, wood-PLA displayed a more uniform deformation at the same strain value (Point II) and a broad plastic deformation range before breakage (Point III), as shown in Figure 4C. Due to the plastic deformation in wood-PLA, the strain energy density (see Equation (2)) of wood-PLA reached 8.91×10^{-7} J/m^3, which is 1.41 times greater than that of the PLA sample. These findings are consistent with other studies on wood fiber-PLA and biofibre-reinforced PLA composites. Lage-Rivera et al. observed that increasing fiber content led to a progressive decrease in tensile strength [22], whereas the elongation at break increased, reaching its maximum at a fiber content of 15%. Siddiqui et al. [58], and Mazur et al. [59] reported the reduction of Young's modulus of wood-PLA. Similarly, Yu et al. confirmed these observations in their work [60].

The higher strain energy density observed in wood–PLA composites may be attributed to several synergistic mechanisms. Interfacial debonding between the wood fibers and the PLA matrix, followed by fiber pull-out, serves as an effective energy dissipation process. In addition, the introduction of wood particles results in a heterogeneous internal structure that disrupts crack propagation paths, increases the effective crack path length, and reduces local stress concentrations. These combined effects delay the onset of catastrophic failure, enabling the material to accommodate greater deformation prior to fracture.

The reduction in the ultimate tensile strength and Young's modulus results from the introduction of the wood fiber. According to Tao's research [61], wood fiber has a polar (hydrophilic) surface, whereas PLA has a non-polar (hydrophobic) surface. The disparity between the polar and non-polar surfaces prevents the formation of a strong interfacial bond [62]. During the tensile test, the pull-out effects are often observed in on the wood-PLA samples in previous studies [12]. Besides, many researchers have found that short fiber reinforcement can reduce the tensile strength of polymers, as these fibers cannot effectively bear tensile loads the way continuous molecular chains do [13, 63].

In addition to the interfacial challenges caused by the wood fibers, thermomechanical degradation of the PLA matrix during melt processing can also play a significant role in reducing the mechanical performance of wood-PLA composites [64]. During compounding and extrusion, repeated heating and shearing may induce chain scissions in the PLA, leading to decreased molecular weight, which in turn compromises the thermal stability and mechanical integrity of the material [65]. These degradative changes are often accompanied by an increase in crystallinity, as shorter polymer chains reorganize more easily [66].

3.1.3 | SENB Test of PLA and Wood-PLA

3.1.3.1 | Fracture Pattern. Figure 5 exhibits the crack initiation and propagation of PLA and wood-PLA samples during SENB tests. The contour diagrams illustrate the evolution of the ε_{xx} strain during the loading processes. For the PLA sample, crack initiation occurred at the notch tip, followed by an increasingly pronounced crack propagation as the applied displacement increased. The observed strain distribution indicates that stress was concentrated around the notch tip, resulting in brittle fracture characteristics with a straight, upward crack propagation. Notably, samples with a 4 mm notch length exhibited more pronounced cracking under the same applied displacement due to the larger maximum stress at the crack tip. The maximum flexural stress in SENB samples is approximately calculated in Supporting Information using a simplified three-point bending model. It shows that the maximum flexural stress decreases as the notch length increases under the same deflection.

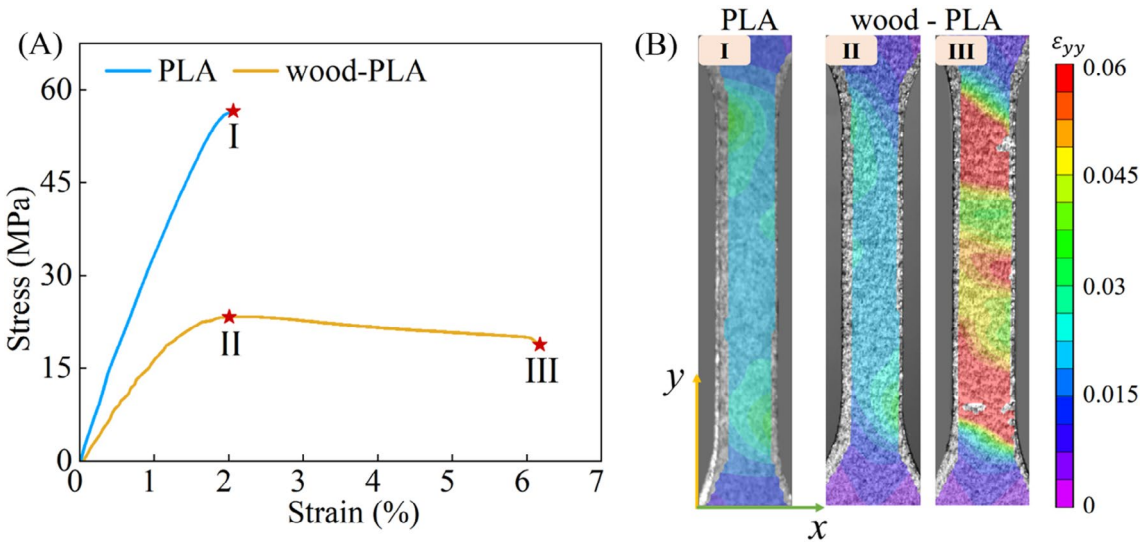

FIGURE 4 | The tensile results of PLA and wood-PLA samples in the control group: (A) stress–strain curves, (B) ε_{yy} strain contour of the PLA and wood-PLA samples at critical displacement (Marked on red stars in (A)).

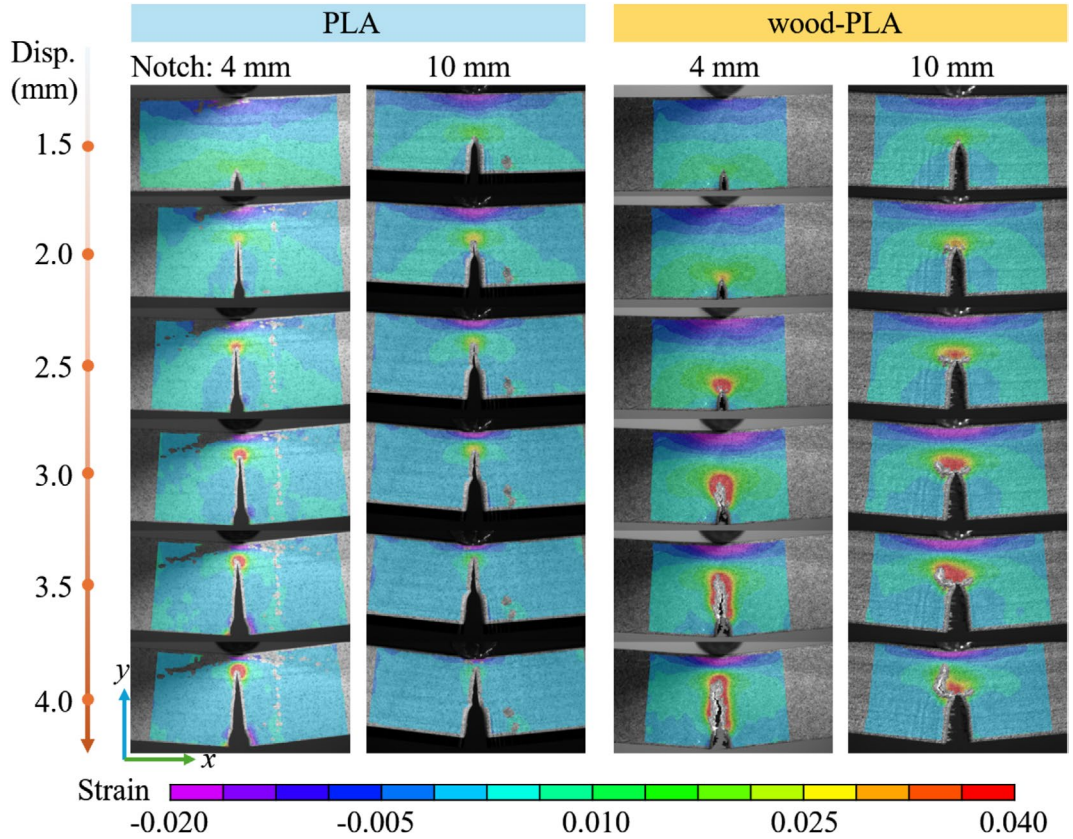

FIGURE 5 | The ε_{xx} contour diagram of PLA and wood-PLA SENB samples with 4 and 10 mm notch length during the loading process.

Due to the introduction of wood fibers, wood-PLA samples exhibited a different crack evolution pattern, which was impacted by the notch length. The presence of wood fibers led to more distributed plastic strain accumulation around the crack tip, as highlighted in the red areas (Figure 5), which was consistent with the observation in Section 3.1.2 that wood-PLA exhibited more plastic deformation before break. The sample with a 4 mm notch exhibited a slight zigzag crack pattern, with the propagation primarily in the vertical direction. In contrast, the 10 mm notched wood-PLA sample showed horizontal crack propagation before the applied displacement reached 3 mm. This behavior was attributed to the lower maximum flexural stress at the notch tip compared to the 4 mm notched sample, which inhibited the initial upward crack propagation. Instead, the strain

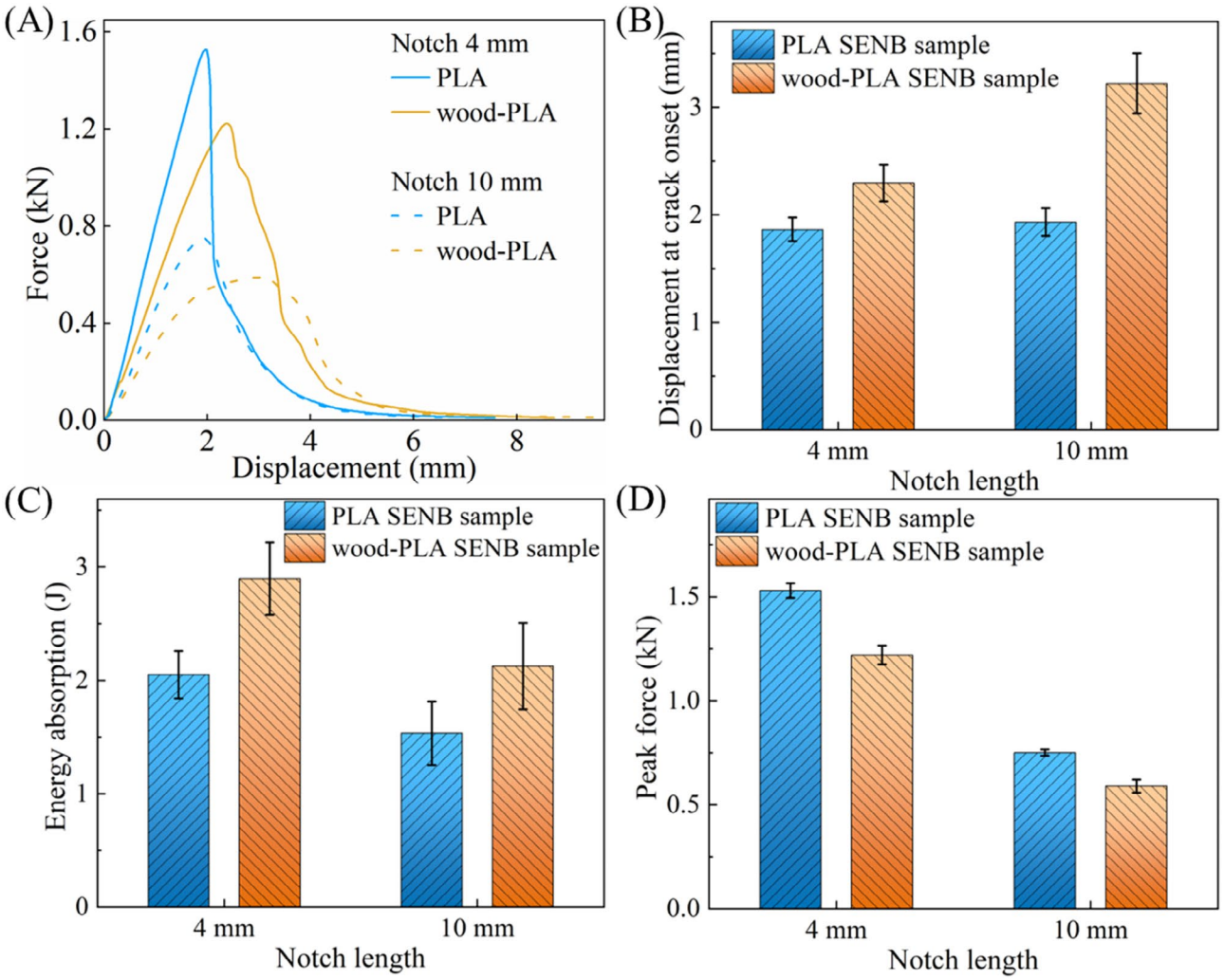

FIGURE 6 | Results of SENB samples in the control group: (A) force-displacement curves, (B) displacement at crack onset, (C) energy absorption, and (D) peak force. The displacement at crack onset of wood-PLA with a 10 mm notch corresponds to the vertical crack onset.

mismatch between the elongated region above the notch tip and the undeformed material below led to interlayer shear debonding, causing the crack to propagate horizontally at first. After the applied displacement exceeded 3 mm, the crack changed its direction and developed vertically upwards due to the tensile stress.

3.1.3.2 | Force-Displacement Curve. Figure 6A presents force-displacement curves obtained from SENB samples with notch lengths of 4 and 10 mm. PLA samples exhibited a higher initial peak force, followed by a sharp load drop, characteristic of brittle fracture. In contrast, wood-PLA samples displayed a lower peak force but a more gradual force decline, corresponding to the ductile fracture mode in Figure 5.

For the 4 mm notched samples (Figure 6B), wood-PLA exhibited a larger displacement at crack onset compared to PLA, measuring 2.3 mm. For the 10 mm notched samples, the wood-PLA sample initially developed a horizontal crack at a displacement of 2.1 mm, followed by vertical crack propagation beginning at 3.2 mm. During the debonding phase from 2.1 to 3.2 mm, no significant force reduction was observed in wood-PLA.

Figure 6C shows that wood-PLA samples exhibited higher energy absorption compared to PLA. The energy absorption of wood-PLA was 2.90 J for the 4 mm notched samples and 2.13 J for the 10 mm notched samples, whereas the corresponding values for PLA counterparts were 2.05 and 1.53 J, respectively. In Figure 6D, PLA exhibited a significantly higher peak force of 1.53 kN with the 4 mm notch, which decreased to 1.23 kN with the 10 mm notch. In contrast, the peak force for wood-PLA samples was only 0.75 and 0.59 kN for the 4 and 10 mm notched samples, respectively, confirming the lower strength of wood-PLA. Hence, despite its lower strength, wood-PLA exhibited superior energy absorption capability and ductile fracture characteristics, preventing sudden failure under loading.

3.2 | Water Absorption and Thermal Analysis

3.2.1 | Water Absorption Ability

The wood-PLA tensile samples exhibit a significantly higher water absorption rate compared to the pure PLA samples. Figure 7A exhibits that after soaking for 3 days, the water absorption rate of wood-PLA reached 5.24%, which was 12.8

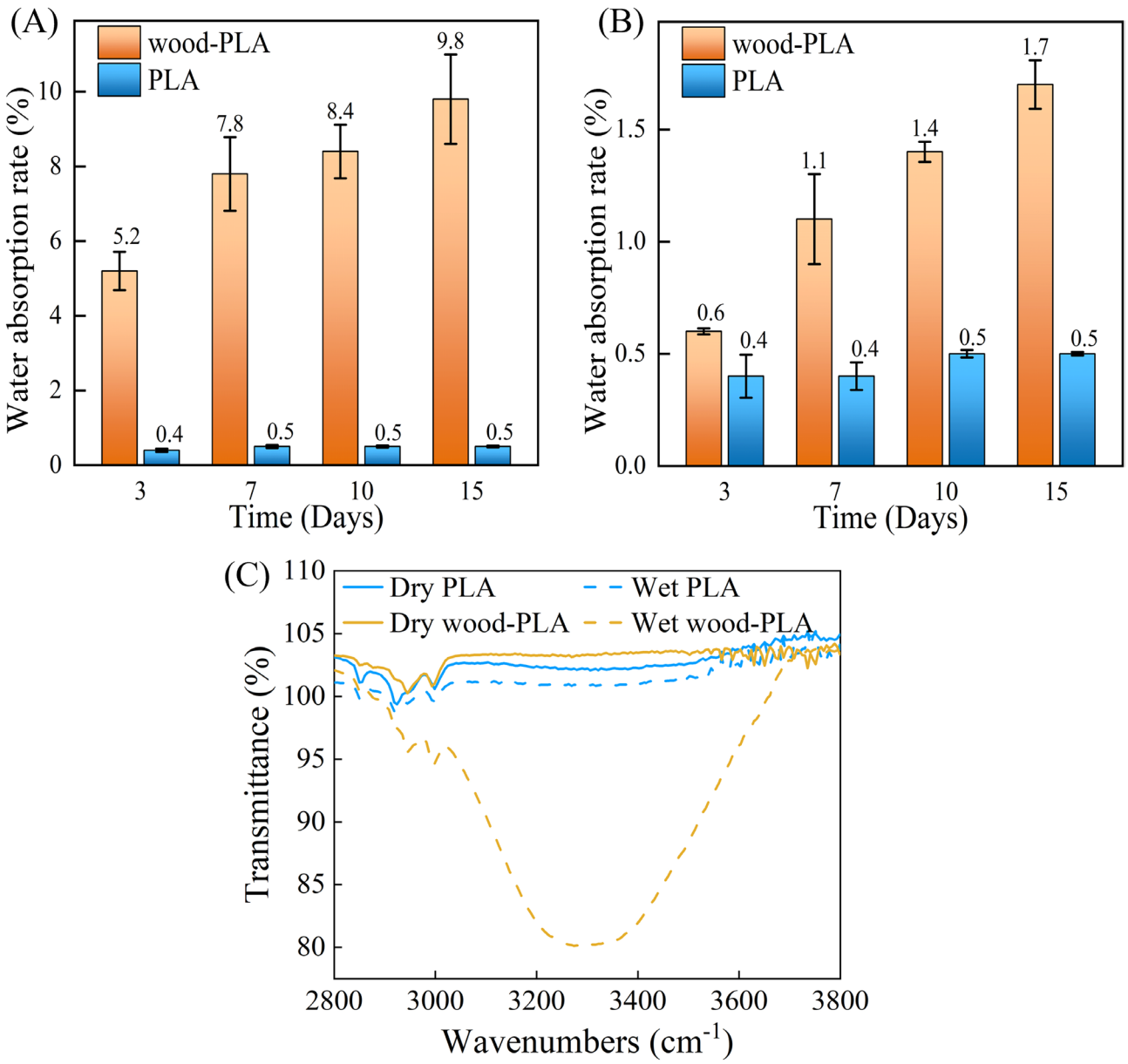

FIGURE 7 | (A) The water absorption rates of wood-PLA and PLA tensile samples, (B) SENB samples, (C) ATR-FTIR spectra of PLA and wood-PLA samples after drying and after 7 days of water immersion.

times higher than that of PLA (0.41%). Thereafter, the water absorption rate of wood-PLA continued to increase significantly with immersion time, whereas the increase in PLA remained negligible. Notably, after 15 days of immersion, the water absorption rate of the wood-PLA samples rose to 9.81%, which was 21.7 times higher than that of the PLA samples (0.45%). The high water absorption in wood-PLA arises from the hydrophilic nature of wood fibers, where the cellulose composition promotes interactions with water molecules [22]. The ATR-FTIR results [67, 68] in Figure 7C show that the wood-PLA exhibited a pronounced increase in the peak intensity within the wavenumber range of 3000–4000 cm^{-1} (with transmittance reaching approximately 80%) after water immersion, whereas PLA showed no significant change. The pronounced peak in this region indicates an increased presence of hydroxyl groups, which reflects the enhanced formation of hydrogen bonds and the uptake of water molecules within the wood-PLA composites [55].

In SENB samples (Figure 7B), PLA maintained consistently low values (around 0.44%) with minimal change over time. However, the values of wood-PLA were significantly lower than those of their tensile counterparts, despite exhibiting a similar increasing trend over time, with a maximum value of 1.72% at 15 days. The reduction observed in SENB samples was caused by their increased thickness, as well as differences in shape and surface area, which reduced their overall contact efficiency with water. Additionally, the greater thickness likely hindered water penetration into the inner layers, resulting in a lower absorption rate over the same immersion duration.

Pure PLA exhibits relatively poor hydrophilicity, particularly on the smooth surfaces of PLA materials produced by traditional manufacturing methods [18, 35]. Although using FDM can effectively enhance hydrophilicity by creating surface porosities and uneven, wavy textures that increase contact with

water [69], the water absorption of FDM printed PLA is still limited.

3.2.2 | Effect of Water Absorption on Thermal Properties

Figure 8A presents the DSC thermograms of PLA and wood-PLA in both dry and wet states. The glass transition temperature (T_g) of dry PLA was measured at 58.8°C, indicating that water absorption had only a marginal effect on the polymer chain mobility of neat PLA. In contrast, dry wood-PLA exhibited a lower T_g of 57.2°C, which further decreased to 55.5°C after moisture absorption. This more pronounced reduction highlights the effect of water absorption on wood particles in wood-PLA, which enhances segmental motion and lowers the glass transition temperature.

The TG results shown in Figure 8B reveal that the major weight loss for all samples occurred between 300°C and 400°C, corresponding to the thermal decomposition of the PLA matrix. The wet wood-PLA displayed a slight shift of the TG and DTG curves toward lower temperatures, suggesting the evaporation of absorbed moisture retained by the hydrophilic wood fibers. In contrast, wet PLA showed negligible weight loss in this region due to its much lower water uptake. Importantly, the decomposition profiles of wet and dry samples after 15 days of immersion at room temperature exhibited no notable differences, indicating that no measurable degradation had taken place during this period.

3.3 | Tensile Properties With Water Immersion

3.3.1 | Stress–Strain Curves

Figure 9 presents the tensile stress–strain curves of PLA and wood-PLA after different immersion durations. Additionally, it compares the curves of samples that were re-dried after each immersion stage, providing insights into the effects of water

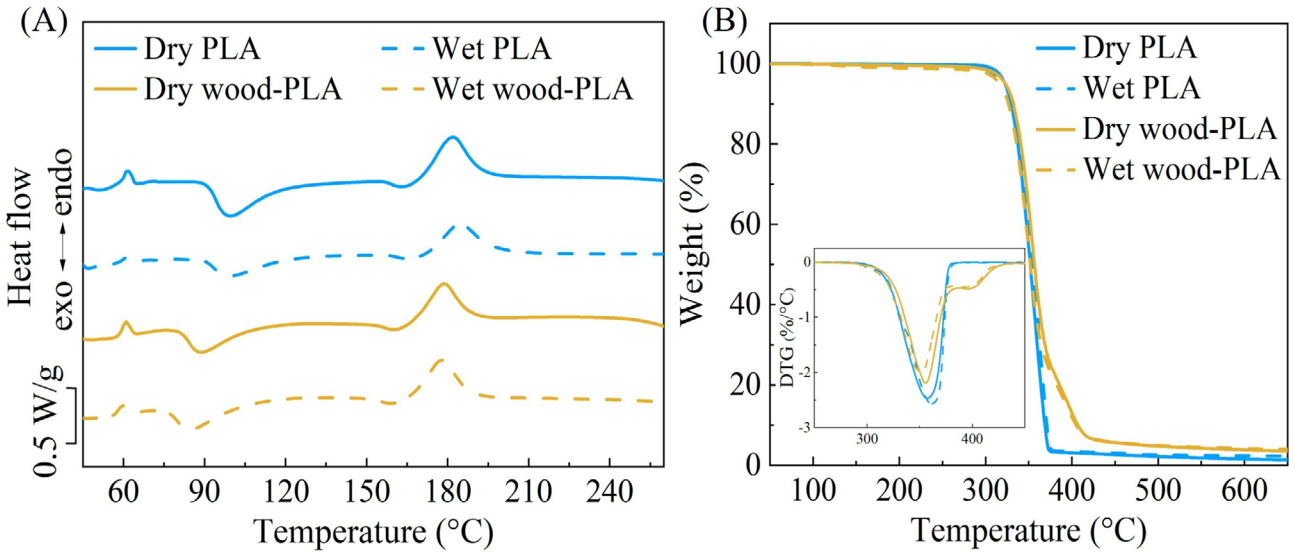

FIGURE 8 | Thermal analysis curves from (A) DSC tests and (B) TGA tests.

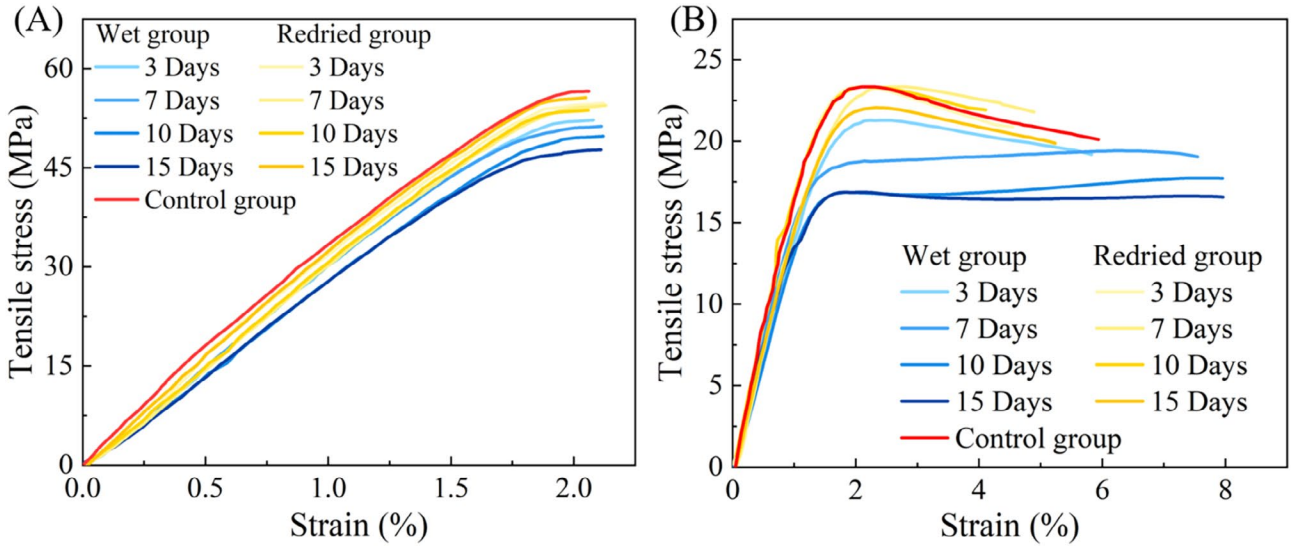

FIGURE 9 | The stress–strain curves of (A) PLA and (B) wood-PLA with different conditions.

exposure on the mechanical properties of the materials. It can be observed that prolonged immersion led to a decline in tensile strength and stiffness for both materials in the wet group. Wood-PLA exhibited a more pronounced reduction in tensile strength due to its higher hydrophilicity. In the wet group, the elongation at break of wood-PLA increased significantly after 7 days of water exposure. The re-dried samples showed notable recovery in their tensile stress–strain behavior, indicating that the observed degradation was primarily physical and reversible, rather than a result of permanent chemical breakdown. Both wet and re-dried groups exhibited the same deformation and fracture patterns shown in Figure 4B.

3.3.2 | Mechanical Properties

The ultimate tensile strength, elastic modulus, elongation at break, and strain energy density were extracted from tensile stress–strain curves and presented in Figure 10. The mechanical metrics of control group samples were plotted as dashed lines for comparison. As shown in Figure 10A, the ultimate tensile strength notably decreased as the water immersion duration increased from 3 to 15 days. The ultimate tensile strength of PLA samples dropped from 54.6 MPa in the control group to 47.8 MPa after 12 days of immersion, demonstrating a 12% reduction. The ultimate tensile strength of wood-PLA samples decreased from 23.4 MPa in the control group to 21.1 MPa after 3 days, further dropping to 18.5 MPa after 15 days, representing a 20% reduction. For both PLA and wood-PLA samples, the most significant decrease in ultimate tensile strength occurred within the first 7 days, after which the decline gradually stabilized. By applying the Jonckheere–Terpstra test [54] to the ultimate tensile strength of wood-PLA and PLA after water immersion, both datasets were shown to exhibit a clear monotonic decreasing trend. The one-sided p values were 0.998 and 0.982, respectively, for wood-PLA and PLA, both exceeding the significance threshold of 0.95. After redrying, the tensile strength of both samples returned almost to the control level.

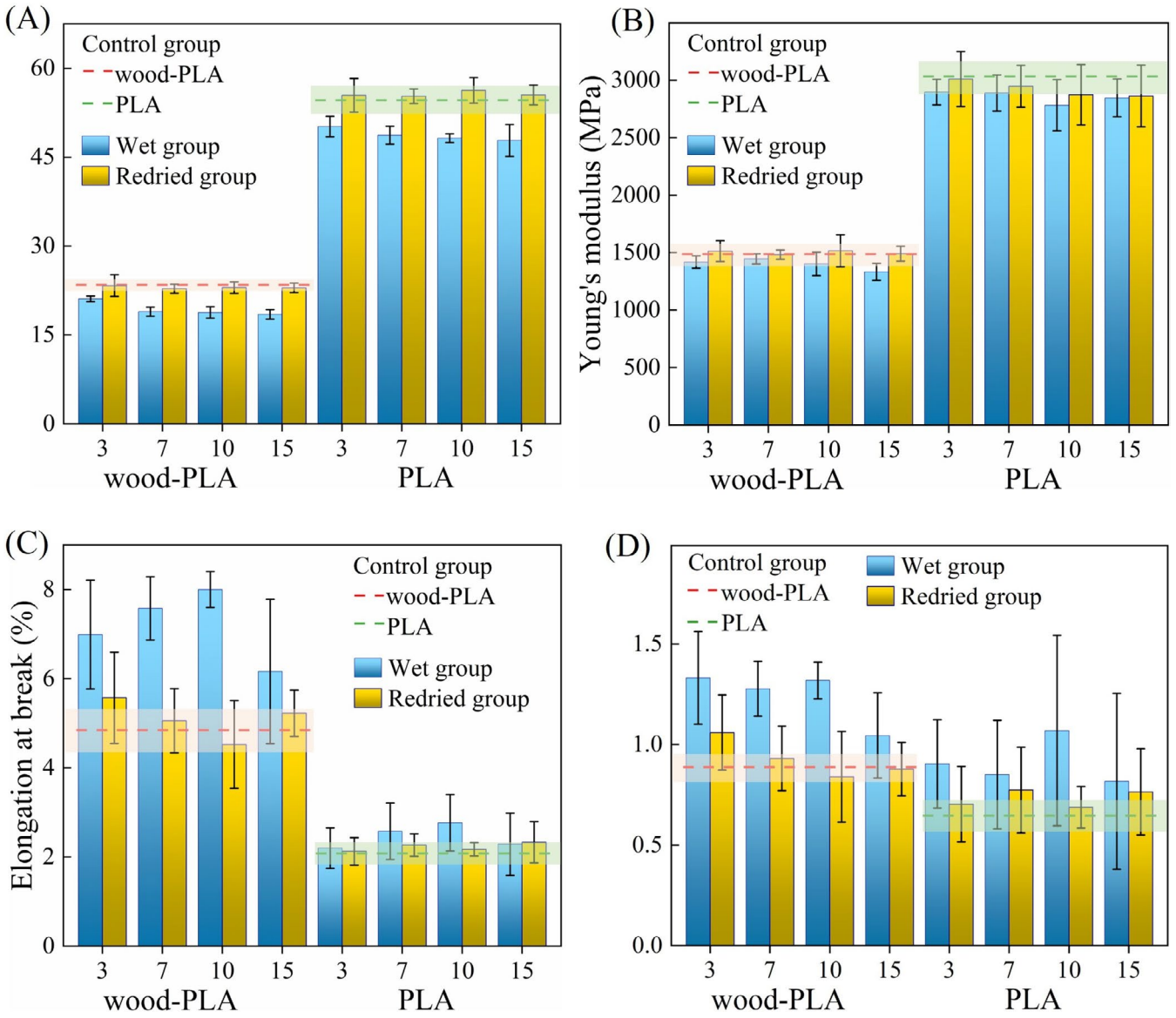

FIGURE 10 | Tensile results of wet and redried groups: (A) ultimate tensile strength, (B) Young's modulus, (C) elongation at break, and (D) strain energy density.

Figure 10B shows that in the wet group, Young's modulus of wood-PLA decreased with prolonged immersion, dropping from 1495 MPa in the control group to 1333 MPa after 15 days, corresponding to a 10% reduction. After redrying, the Young's modulus of the samples from each immersion stage returned to its original value. PLA samples exhibited a decrease from 3102 to 2846 MPa after 15 days of water exposure, representing an 8% decrease. The Young's modulus of PLA samples immersed for 3 days fully recovered to its initial value after redrying. However, for other immersion durations, the redried samples exhibited a lower modulus than the initial value. After 15 days of immersion, the Young's modulus of the redried samples was 2863 MPa.

Water absorption had a significant influence on elongation at break. As shown in Figure 10C, with increasing immersion time, both PLA and wood-PLA samples exhibited a notable increase in elongation at break, reaching a peak value at 10 days, followed by a decline by 15 days. The wood-PLA sample had an initial elongation at break of 4.8% in the control group, reaching a peak of 8.0% after 10 days, representing a 66% increase. For PLA, the value started at 2.1% and peaked at 2.8% after 10 days. By applying the Jonckheere–Terpstra test to the elongation at break of wood-PLA and PLA after water immersion, with particular focus on the datasets for 3, 7, and 10 days of immersion, both materials were found to exhibit a clear monotonic increasing trend. The p values were 0.026 and 0.037, respectively, for wood-PLA and PLA, both below the significance threshold of 0.05. After redrying, the elongation at break of wood-PLA samples decreased compared to the wet group but remained higher than the control group, possibly due to residual moisture trapped within the wood fibers. However, the elongation of PLA returned close to the control level after redrying, suggesting a fully reversible effect in PLA.

Primarily due to the increase of elongation at break, both wood-PLA and PLA samples exhibited an increased energy absorption after water immersion as shown in Figure 10D. Initially, the strain energy density of wood-PLA and PLA was 8.91×10^{-7} J/m^3 and 6.39×10^{-7} J/m^3, respectively. After 10 days of immersion, the strain energy density of the wood-PLA and PLA samples peaked at 1.32×10^{-6} J/m^3 and 8.46×10^{-7} J/m^3, and with the maximum increase rate 48% and 32% respectively. Then, the values for both materials decreased to 9.78×10^{-7} J/m^3 for wood-PLA and 6.87×10^{-7} J/m^3 for PLA, though both remained higher than their initial values. Hence, both wood-PLA and PLA demonstrated a noticeable increase in their energy absorption capacities within a short period (up to 15 days) of water absorption. After redrying, both samples showed a decline in strain energy density, with their values closely aligning with that of control group, indicating that the energy absorption capacity was reversible during the water soaking and redrying treatment processes.

Similar observations have been reported in previous studies on wood-PLA and other biofibre-reinforced PLA composites after water immersion. For instance, Ecker et al. [35] found that immersion in water led to a noticeable reduction in tensile strength, particularly in composites containing higher hydrophilic fiber content. Ayrilmis et al. [16] similarly reported that water uptake caused a pronounced reduction in tensile strength in wood-PLA. Ali et al. [70] emphasized the significant increase in elongation at break and toughness of flax/PLA composites.

The observed changes in mechanical properties can be attributed to water-induced plasticisation [71]. Water functions as an external plasticizer by reducing intermolecular interactions and enhancing chain mobility [72]. Although both PLA and wood-PLA underwent this process, the effect was more pronounced in wood-PLA owing to its hydroxyl-rich constituents (i.e., cellulose and hemicellulose) and higher porosity, which facilitated water uptake and hydrogen bond formation, as discussed in Section 3.2. FTIR analysis corroborated this mechanism, showing intensified absorption in the 3000–4000 cm^{-1} regions after immersion, indicative of increased hydroxyl groups and hydrogen bonding.

3.4 | SENB Test Results With Water Immersion

Figure 11A,C show the force-displacement curves for wood-PLA with 4 and 10 mm notches, respectively. Unlike the tensile results, water absorption had a negligible impact on the peak force of SENB samples. Compared to the curves of the redried samples, the wet samples consistently exhibited a slower force decline stage with higher force levels after the peak force. In contrast, Figure 11E presented that for PLA with a 4 mm notch, regardless of the immersion time or whether the sample was redried, the curves were tightly clustered with very minimal differences. The deformation and fracture patterns remained consistent with the control group as presented in Figure 5, regardless of the water immersion.

As shown in Figure 11B,D, wood-PLA samples with a 4 mm notch exhibited an initial energy absorption of 2.89 J in the control group, which increased to 3.33 J after 15 days of water immersion. Similarly, wood-PLA samples with a 10 mm notch had a slightly lower energy absorption of 2.12 J but increased to 2.89 J by 15 days. Both types of wood-PLA samples exhibited a significant increase in energy absorption: the 4 mm notch sample showed a growth rate of 15%, whereas the 10 mm notch sample demonstrated an even more pronounced increase of 36%. The increase in energy absorption was primarily reflected in the descending phase of the force-displacement curves. As mentioned earlier, compared to the redried samples, the wet samples consistently exhibited a more gradual force decline while maintaining higher force levels after reaching the peak force. Consequently, the area beneath the curves for the wet samples was larger, resulting in greater energy absorption. After redrying, both samples exhibited a reduction in energy absorption, with the values returning to their original level as indicated by the control group.

In contrast, the pure PLA samples showed minimal changes in energy absorption after water immersion, as demonstrated in Figure 11F. The energy values remained stable around 2.1 J, with only slight fluctuations observed. The subtle changes observed in the PLA SENB test can be attributed to the structural characteristics of the SENB testing method. Unlike the dog bone samples used in the tensile test, the SENB configuration exhibited reduced contact efficiency with the surrounding water. The increased thickness of the sample hindered water penetration

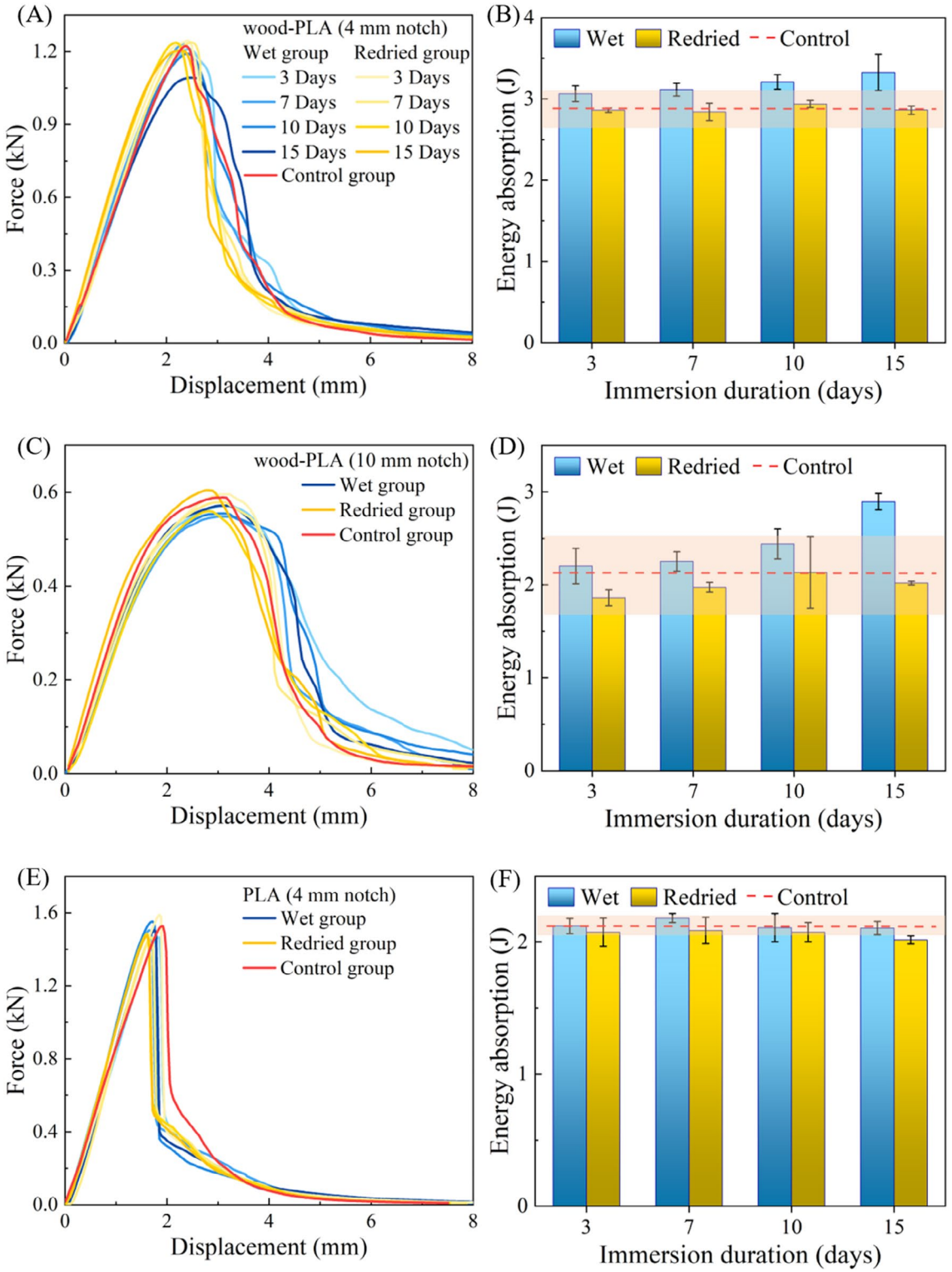

FIGURE 11 | The force-displacement curve and energy absorption of the SENB sample with different conditions: (A) and (B) wood-PLA with 4 mm notch, (C) and (D) wood-PLA with 10 mm notch, (E) and (F) PLA with 4 mm notch.

(mentioned in Figure 7B before), limiting the water absorption effect on the material [18]. This reduction in water absorption was noted in both PLA and wood-PLA samples. Additionally, the minimal variation in energy absorption observed for PLA in the SENB test, compared to wood-PLA, can be explained by the inherent material differences. PLA is less sensitive to water exposure than wood-PLA, which incorporates wood fibers.

The short-term yet non-negligible effects of water immersion on wood–PLA composites carry important implications for their practical use. Due to the hydrophilic nature of wood fibers, these materials readily absorb moisture in humid environments, which can compromise their mechanical performance. As a result, careful consideration must be given when employing such composites in conditions where humidity fluctuates or where

direct water exposure is likely, as their structural reliability may be adversely affected.

At the same time, the observed increase in strain energy density following moisture uptake points to potential utility in applications that demand enhanced energy absorption, such as impact resistance or vibration damping. Nonetheless, the associated reduction in tensile strength must be taken into account to ensure that the material's load-bearing capacity remains suitable for its intended function.

Encouragingly, the recovery of mechanical properties after redrying suggests that the degradation induced by short-term water exposure is largely physical and reversible. This characteristic is particularly beneficial in scenarios where the material may intermittently come into contact with moisture, as its performance can be restored through appropriate drying, thereby prolonging the service life of the composite.

4 | Conclusions

This study examined the mechanical properties of wood-PLA composites manufactured via FDM printing under water conditioning. Tensile and SENB tests were conducted on wood-PLA and compared with those of pure PLA. The impact of water absorption on mechanical performance was evaluated through water immersion for up to 15 days, followed by a redrying process. The key findings are as follows:

Before water immersion, wood-PLA exhibited a significantly lower ultimate tensile strength (23.4 MPa) than pure PLA (54.6 MPa) but a 41% higher strain energy density (8.91×10^{-7} J/m^3 compared with 6.31×10^{-7} J/m^3). The longer elongation at break in wood-PLA contributes to its higher energy absorption capacity. Similar trends were observed in SENB testing, where wood-PLA consistently absorbed more energy. This improvement in energy absorption was attributed to the introduction of wood fibers, which altered the fracture behavior and shifted the brittle failure observed in PLA to ductile fracture.

During water immersion, both materials experienced a decline in tensile strength and an increase in energy absorption capacity. These changes resulted from the plasticization effect induced by water molecules, which acted as external plasticizers by penetrating the polymer matrix and temporarily disrupting intermolecular interactions. Moreover, wood-PLA exhibited significant water absorption due to its higher porosity and the presence of hydrophilic components in the wood fibers such as cellulose and hemicellulose. Although the tensile strength and elastic modulus of wood-PLA exhibited a maximum reduction of 20% and 10%, the elongation at break and energy absorption ability for wood-PLA increased by 66% and 48%, respectively.

After drying, both materials largely regained their original properties, including ultimate tensile strength, elongation at break, Young's modulus, and energy absorption capacity. This recovery demonstrated the reversible nature of water-induced plasticisation during short-term water immersion. These findings highlight the potential of FDM printed wood-PLA composites for use in environments with intermittent moisture exposure, provided that adequate drying can be ensured between wet cycles.

In addition to its technical implications, this study has significant potential for broader impact. The findings could benefit industries such as construction, automotive, and packaging, where materials are exposed to variable moisture conditions. Furthermore, this work contributes to the growing body of research in sustainable and bio-based materials, offering insights into the processing and performance of wood-PLA composites in real-world applications. This study paves the way for future research aimed at enhancing the performance and durability of wood-PLA composites, including their long-term behavior in humid environments.

Author Contributions

Weilong Xu: methodology, data curation, investigation, visualization, writing – original draft, formal analysis. **Meiyu Li:** methodology, software, investigation, formal analysis, validation, writing – original draft. **Yanan Xu:** resources, writing – review and editing, data curation, investigation. **Ali Entezari:** writing – review and editing, supervision. **Jianguang Fang:** conceptualization, methodology, project administration, resources, writing – review and editing, supervision, funding acquisition.

Acknowledgments

The last author is a recipient of the Australian Research Council (ARC) Discovery Early Career Research Award (grant no. DE210101676). The support from the ARC is acknowledged. Open access publishing facilitated by University of Technology Sydney, as part of the Wiley - University of Technology Sydney agreement via the Council of Australian University Librarians.

Conflicts of Interest

The authors declare no conflicts of interest.

Data Availability Statement

Data will be made available on request.

References

1. S. Chakraborty and M. C. Biswas, "3D Printing Technology of Polymer-Fiber Composites in Textile and Fashion Industry: A Potential Roadmap of Concept to Consumer," *Composite Structures* 248 (2020): 112562.

2. A. Melocchi, N. Inverardi, M. Uboldi, et al., "Retentive Device for Intravesical Drug Delivery Based on Water-Induced Shape Memory Response of Poly (Vinyl Alcohol): Design Concept and 4D Printing Feasibility," *International Journal of Pharmaceutics* 559 (2019): 299–311.

3. D. K. Yadav, R. Srivastava, and S. Dev, "Design & Fabrication of ABS Part by FDM for Automobile Application," *Materials Today: Proceedings* 26 (2020): 2089–2093.

4. E. Zaneldin, W. Ahmed, A. Mansour, and A. E. Hassan, "Dimensional Stability of 3D Printed Objects Made From Plastic Waste Using FDM: Potential Construction Applications," *Buildings* 11, no. 11 (2021): 516.

5. A. Alfaer, Y. Aljabri, A. Alameer, M. A. Illah, H. Thubab, and A. Thubab, "Applications, Benefits, and Limitations of Fiber-Reinforced

Composites in Fixed Prosthodontics," *International Journal of Community Medicine and Public Health* 10, no. 11 (2023): 4462–4467.

6. N. K. Faheed, "Advantages of Natural Fiber Composites for Biomedical Applications: A Review of Recent Advances," *Emergent Materials* 7, no. 1 (2024): 63–75.

7. M. Heidari-Rarani, M. Rafiee-Afarani, and A. Zahedi, "Mechanical Characterization of FDM 3D Printing of Continuous Carbon Fiber Reinforced PLA Composites," *Composites Part B: Engineering* 175 (2019): 107147.

8. C. Zeng, L. Liu, W. Bian, J. Leng, and Y. Liu, "Bending Performance and Failure Behavior of 3D Printed Continuous Fiber Reinforced Composite Corrugated Sandwich Structures With Shape Memory Capability," *Composite Structures* 262 (2021): 113626.

9. I. Ksouri, N. Guermazi, N. Haddar, and H. F. Ayedi, "Effects of Processing Steps and Hygrothermal Ageing on Mechanical Performance of PA6GF30 Composite: Interfacial Shear Strength," *Polymer Composites* 39, no. 2 (2016): 504–512.

10. L. Cao, J. Xiao, J. K. Kim, and X. Zhang, "Effect of Post-Process Treatments on Mechanical Properties and Surface Characteristics of 3D Printed Short Glass Fiber Reinforced PLA/TPU Using the FDM Process," *CIRP Journal of Manufacturing Science and Technology* 41 (2023): 135–143.

11. S. Rijckaert, L. Daelemans, L. Cardon, M. Boone, W. Van Paepegem, and K. De Clerck, "Continuous Fiber-Reinforced Aramid/PETG 3D-Printed Composites With High Fiber Loading Through Fused Filament Fabrication," *Polymers* 14, no. 2 (2022): 298.

12. T.-C. Yang and C.-H. Yeh, "Morphology and Mechanical Properties of 3D Printed Wood Fiber/Polylactic Acid Composite Parts Using Fused Deposition Modeling (FDM): The Effects of Printing Speed," *Polymers* 12, no. 6 (2020): 1334.

13. H. Bi, Z. Ren, R. Guo, M. Xu, and Y. Song, "Fabrication of Flexible Wood Flour/Thermoplastic Polyurethane Elastomer Composites Using Fused Deposition Molding," *Industrial Crops and Products* 122 (2018): 76–84.

14. N. Gama, A. Ferreira, A. Barros-Timmons, and D. Evtuguin, "Polyamide 6/Modified Pine Bark Particle Composites for Additive Manufacturing," *Journal of Materials Science* 56 (2021): 19093–19105.

15. M. Kariz, M. Sernek, M. Obućina, and M. K. Kuzman, "Effect of Wood Content in FDM Filament on Properties of 3D Printed Parts," *Materials Today Communications* 14 (2018): 135–140.

16. N. Ayrilmis, M. Kariz, J. H. Kwon, and M. Kitek Kuzman, "Effect of Printing Layer Thickness on Water Absorption and Mechanical Properties of 3D-Printed Wood/PLA Composite Materials," *International Journal of Advanced Manufacturing Technology* 102, no. 5-8 (2019): 2195–2200.

17. A. Couture, G. Lebrun, and L. Laperrière, "Mechanical Properties of Polylactic Acid (PLA) Composites Reinforced With Unidirectional Flax and Flax-Paper Layers," *Composite Structures* 154 (2016): 286–295.

18. A. Haryńska, H. Janik, M. Sienkiewicz, B. Mikolaszek, and J. Kucińska-Lipka, "PLA–Potato Thermoplastic Starch Filament as a Sustainable Alternative to the Conventional PLA Filament: Processing, Characterization, and FFF 3D Printing," *ACS Sustainable Chemistry & Engineering* 9, no. 20 (2021): 6923–6938.

19. D. Bajwa, M. Eichers, J. Shojaeiarani, and A. Kallmeyer, "Influence of Biobased Plasticizers on 3D Printed Polylactic Acid Composites Filled With Sustainable Biofiller," *Industrial Crops and Products* 173 (2021): 114132.

20. A. M. S. Marton, F. M. Monticeli, N. C. Zanini, et al., "Revalorization of Australian Royal Palm (*Archontophoenix alexandrae*) Waste as Reinforcement in Acrylonitrile Butadiene Styrene (ABS) for Use in 3D Printing Pen," *Journal of Cleaner Production* 365 (2022): 132808.

21. A. Le Duigou, M. Castro, R. Bevan, and N. Martin, "3D Printing of Wood Fibre Biocomposites: From Mechanical to Actuation Functionality," *Materials and Design* 96 (2016): 106–114.

22. S. Lage-Rivera, A. Ares-Pernas, M. S. Dopico-García, J. Covas, and M. J. Abad, "Comparing Lignin and Spent Coffee Grounds as Bio-Fillers in PLA 3D-Printable Filaments," *Polymer Composites* 45, no. 16 (2024): 14566–14579.

23. Y. Tao, L. Pan, D. Liu, and P. Li, "A Case Study: Mechanical Modeling Optimization of Cellular Structure Fabricated Using Wood Flour-Filled Polylactic Acid Composites With Fused Deposition Modeling," *Composite Structures* 216 (2019): 360–365.

24. R. Periyasamy, M. Hemanth Kumar, S. M. Rangappa, and S. Siengchin, "A Comprehensive Review on Natural Fillers Reinforced Polymer Composites Using Fused Deposition Modeling," *Polymer Composites* 44, no. 7 (2023): 3715–3747.

25. Y. Huang, S. Löschke, and G. Proust, "In the Mix: The Effect of Wood Composition on the 3D Printability and Mechanical Performance of Wood-Plastic Composites," *Composites Part C: Open Access* 5 (2021): 100140.

26. R. Sarker, M. A. A. Bari, S. Saad, et al., "Investigation of Mechanical and Physicochemical Properties of Additively Manufactured Underutilized Wood-PLA Biocomposites," *Polymer Composites* (2025).

27. D. Krapež Tomec and M. Kariž, "Use of Wood in Additive Manufacturing: Review and Future Prospects," *Polymers* 14, no. 6 (2022): 1174.

28. A. Aniskevich, O. Bulderberga, and L. Stankevics, "Moisture Sorption and Degradation of Polymer Filaments Used in 3D Printing," *Polymers* 15, no. 12 (2023): 2600.

29. M. Mohammed, A. J. M. Jawad, A. M. Mohammed, et al., "Challenges and Advancement in Water Absorption of Natural Fiber-Reinforced Polymer Composites," *Polymer Testing* 124 (2023): 108083.

30. H. Ramezani Dana and F. Ebrahimi, "Synthesis, Properties, and Applications of Polylactic Acid-Based Polymers," *Polymer Engineering and Science* 63, no. 1 (2023): 22–43.

31. A. Nicolau, M. A. Pop, and C. Coșereanu, "3D Printing Application in Wood Furniture Components Assembling," *Materials* 15, no. 8 (2022): 2907.

32. E. Estakhrianhaghighi, A. Mirabolghasemi, Y. Zhang, L. Lessard, and A. Akbarzadeh, "3D-Printed Wood-Fiber Reinforced Architected Cellular Composites," *Advanced Engineering Materials* 22, no. 11 (2020): 2000565.

33. M. Kariz, M. Sernek, and M. K. Kuzman, "Effect of Humidity on 3D-Printed Specimens From Wood-PLA Filaments," *Wood Research* 63, no. 5 (2018): 917–922.

34. F. N. Ainin, M. Azaman, M. Abdul Majid, and M. Ridzuan, "The Influence of Water Absorption on the Mechanical Performance of 3D-Printed Sandwich Composite Structures Made From PLA-Based Materials Under Quasi-Static Loading Conditions," *Polymer Composites* 46, no. 7 (2025): 6221–6240.

35. J. V. Ecker, A. Haider, I. Burzic, A. Huber, G. Eder, and S. Hild, "Mechanical Properties and Water Absorption Behaviour of PLA and PLA/Wood Composites Prepared by 3D Printing and Injection Moulding," *Rapid Prototyping Journal* 25, no. 4 (2019): 672–678.

36. H. Oliver-Ortega, Q. Tarrés, P. Mutjé, M. Delgado-Aguilar, J. A. Méndez, and F. X. Espinach, "Impact Strength and Water Uptake Behavior of Bleached Kraft Softwood-Reinforced PLA Composites as Alternative to PP-Based Materials," *Polymers* 12, no. 9 (2020): 2144.

37. N. Ayrilmis, M. Kariž, and M. Kitek Kuzman, "Effect of Wood Flour Content on Surface Properties of 3D Printed Materials Produced From Wood Flour/PLA Filament," *International Journal of Polymer Analysis and Characterization* 24, no. 7 (2019): 659–666.

38. M. A. Azka, S. Sapuan, H. Abral, E. Zainudin, and F. A. Aziz, "An Examination of Recent Research of Water Absorption Behavior of Natural Fiber Reinforced Polylactic Acid (PLA) Composites: A Review," *International Journal of Biological Macromolecules* 268 (2024): 131845.

39. M. N. Ahmad, M. R. Ishak, N. A. Maidin, and M. S. Saharudin, "Water Absorption Analysis of Oil Palm Fibre Reinforced Acrylonitrile Butadiene Styrene Composites by Fick's Law," *Journal of Advanced Research in Experimental Fluid Mechanics and Heat Transfer* 20, no. 1 (2025): 150–158.

40. J. A. Martínez-Sánchez, P. E. Romero, F. Comino, E. Molero, and M. Ruiz de Adana, "Effect of Material Extrusion Process Parameters to Enhance Water Vapour Adsorption Capacity of PLA/Wood Composite Printed Parts," *Polymers* 16, no. 20 (2024): 2934.

41. C. Zandvliet, N. Bandyopadhyay, and D. Ray, "Water Absorption of Jute/Polylactic Acid Composite Intended for an Interior Application and Comparison With Wood-Based Panels," *Journal of the Institution of Engineers (India): Series D* 95 (2014): 49–55.

42. S. A. Sajjadi, F. A. Ghasemi, P. Rajaee, and M. Fasihi, "Evaluation of Fracture Properties of 3D Printed High Impact Polystyrene According to Essential Work of Fracture: Effect of Raster Angle," *Additive Manufacturing* 59 (2022): 103191.

43. Nanovia, "Nanovia PLA EF—Electrostatic Discharge (ESD) Safe PLA Filament," accessed 5 August, 2025, https://nanovia.tech/en/ref/nanovia-pla-ef/.

44. International A, "Standard Test Method for Tensile Properties of Plastics.Vol D638," (2022).

45. A. Moetazedian, A. Gleadall, X. Han, and V. V. Silberschmidt, "Effect of Environment on Mechanical Properties of 3D Printed Polylactide for Biomedical Applications," *Journal of the Mechanical Behavior of Biomedical Materials* 102 (2020): 103510.

46. M. Li, Y. Xu, and J. Fang, "Orthotropic Mechanical Properties of PLA Materials Fabricated by Fused Deposition Modeling," *Thin-Walled Structures* 199 (2024): 111800.

47. S. Linforth, T. Ngo, P. Tran, D. Ruan, and R. Odish, "Investigation of the Auxetic Oval Structure for Energy Absorption Through Quasi-Static and Dynamic Experiments," *International Journal of Impact Engineering* 147 (2021): 103741.

48. J. R. C. Dizon, A. H. Espera, Jr., Q. Chen, and R. C. Advincula, "Mechanical Characterization of 3D-Printed Polymers," *Additive Manufacturing* 20 (2018): 44–67.

49. International A, "Standard Test Methods for Plane-Strain Fracture Toughness and Crack Propagation of Plastics. Vol D5045," (2021).

50. International A, "Standard Test Method for Measurement of Fracture Toughness," E1820, (2021).

51. T. Li, Y. Chen, and L. Wang, "Enhanced Fracture Toughness in Architected Interpenetrating Phase Composites by 3D Printing," *Composites Science and Technology* 167 (2018): 251–259.

52. O. Lampron, A. Lingua, D. Therriault, and M. Lévesque, "Characterization of the Non-Isotropic Tensile and Fracture Behavior of Unidirectional Polylactic Acid Parts Manufactured by Material Extrusion," *Additive Manufacturing* 61 (2023): 103369.

53. International A, "ASTM D570-22: Standard Test Method for Water Absorption of Plastics. Vol D570-22, West Conshohocken, PA, ASTM International," (2022).

54. A. Al Aita, M. Aslam, and F. Smarandache, "Jonckheere Trend Test Under Indeterminacy With Applications," *International Journal of Analysis and Applications* 22 (2024): 130.

55. D. M. Mamand, J. M. Hadi, R. A. Omer, and S. B. Aziz, "FTIR, UV-VIS, and DFT Approach to Study the Structural, Optical and Thermal Properties of Chitosan Biopolymer," *Doklady Physical Chemistry* 518 (2024): 137–154.

56. R. Kotsilkova and S. Tabakova, "Exploring Effects of Graphene and Carbon Nanotubes on Rheology and Flow Instability for Designing Printable Polymer Nanocomposites," *Nanomaterials* 13, no. 5 (2023): 835.

57. V. K. Balla, K. H. Kate, J. Satyavolu, P. Singh, and J. G. D. Tadimeti, "Additive Manufacturing of Natural Fiber Reinforced Polymer Composites: Processing and Prospects," *Composites Part B: Engineering* 174 (2019): 106956.

58. V. U. Siddiqui, J. Yusuf, S. Sapuan, M. Z. Hasan, M. M. Mudah Bistari, and Z. G. Mohammadsalih, "Mechanical Properties and Flammability Analysis of Wood Fiber Filled Polylactic Acid (PLA) Composites Using Additive Manufacturing," *Journal of Natural Fibers* 21, no. 1 (2024): 2409868.

59. K. E. Mazur, A. Borucka, P. Kaczor, et al., "Mechanical, Thermal and Microstructural Characteristic of 3D Printed Polylactide Composites With Natural Fibers: Wood, Bamboo and Cork," *Journal of Polymers and the Environment* 30, no. 6 (2022): 2341–2354.

60. I. K. Yu, O. Y. Chan, Q. Zhang, L. Wang, K.-H. Wong, and D. C. Tsang, "Upcycling of Spent Tea Leaves and Spent Coffee Grounds Into Sustainable 3D-Printing Materials: Natural Plasticization and Low-Energy Fabrication," *ACS Sustainable Chemistry & Engineering* 11, no. 16 (2023): 6230–6240.

61. Y. Tao, H. Wang, Z. Li, P. Li, and S. Q. Shi, "Development and Application of Wood Flour-Filled Polylactic Acid Composite Filament for 3D Printing," *Materials* 10, no. 4 (2017): 339.

62. M. S. Pp, J. Pitchaimani, and M. Doddamani, "A Short Banana Fiber—PLA Filament for 3D Printing: Development and Characterization," *Polymer Composites* 46, no. 6 (2025): 4863–4880.

63. B. Akhoundi, A. H. Behravesh, and A. Bagheri Saed, "Improving Mechanical Properties of Continuous Fiber-Reinforced Thermoplastic Composites Produced by FDM 3D Printer," *Journal of Reinforced Plastics and Composites* 38, no. 3 (2018): 99–116.

64. P. Zhao, C. Rao, F. Gu, N. Sharmin, and J. Fu, "Close-Looped Recycling of Polylactic Acid Used in 3D Printing: An Experimental Investigation and Life Cycle Assessment," *Journal of Cleaner Production* 197 (2018): 1046–1055.

65. F. Beltrán, V. Lorenzo, J. Acosta, M. De La Orden, and J. M. Urreaga, "Effect of Simulated Mechanical Recycling Processes on the Structure and Properties of Poly (Lactic Acid)," *Journal of Environmental Management* 216 (2018): 25–31.

66. F. Beltrán, V. Lorenzo, M. U. De la Orden, and J. Martínez-Urreaga, "Effect of Different Mechanical Recycling Processes on the Hydrolytic Degradation of Poly (L-Lactic Acid)," *Polymer Degradation and Stability* 133 (2016): 339–348.

67. M. A. Cuiffo, J. Snyder, A. M. Elliott, N. Romero, S. Kannan, and G. P. Halada, "Impact of the Fused Deposition (FDM) Printing Process on Polylactic Acid (PLA) Chemistry and Structure," *Applied Sciences* 7, no. 6 (2017): 579.

68. W. J. Grigsby, M. Gaugler, and D. Torayno, "Understanding the PLA–Wood Adhesion Interface for the Development of PLA-Bonded Softwood Laminates," *Fibers* 10, no. 6 (2022): 51.

69. S. A. Tronvoll, T. Welo, and C. W. Elverum, "The Effects of Voids on Structural Properties of Fused Deposition Modelled Parts: A Probabilistic Approach," *International Journal of Advanced Manufacturing Technology* 97 (2018): 3607–3618.

70. A. Avci, A. A. Eker, M. S. Bodur, and Z. Candan, "Water Absorption Characterization of Boron Compounds-Reinforced PLA/Flax Fiber Sustainable Composite," *International Journal of Biological Macromolecules* 233 (2023): 123546.

71. E. Langer, K. Bortel, S. Waskiewicz, and M. Lenartowicz-Klik, "Assessment of Traditional Plasticizers," in *Plastics Design Library,*

Plasticizers Derived From Post-Consumer PET (William Andrew Publishing, 2020), 1–11.

72. H. Lim and S. W. Hoag, "Plasticizer Effects on Physical–Mechanical Properties of Solvent Cast Soluplus Films," *AAPS PharmSciTech* 14 (2013): 903–910.

Supporting Information

Additional supporting information can be found online in the Supporting Information section. **Figure S1:** Approximate calculation diagram of flexural stress in SENB samples.